Supplementary Information

CoVID-19 Spike Protein Induced Doping and Phononics in Antibody-Coupled-Graphene: Avenue for Viral Detection Application

Ngoc Hoang Lan Nguyen[1], Sungjoon Kim[1], Garrett Lindemann[2], and Vikas Berry[1,*]

1 Department of Chemical Engineering, University of Illinois at Chicago, 929 W Taylor Street, Chicago, Illinois 60607, USA
2 Ramaco LLC, 1101 Sugarview Drive, Sheridan, Wyoming 82801, USA
Corresponding Author: *vikasb@uic.edu

S1. Amino Acids Sequences

Amino Acids	Abbreviation		General form: $H_3N^+ - CH(R) - COO^-$ Linear Formula of R-group
	Three-letter	One letter	
Alanine	Ala	A	CH_3 -
Arginine	Arg	R	$HN=C(NH_2)-NH-(CH_2)_3$ -
Asparagine	Asn	N	$H_2N-CO-CH_2$ -
Aspartate	Asp	D	$HOOC-CH_2$ -
Cysteine	Cys	C	$HS-CH_2$ -
Glutamate	Glu	E	$HOOC-(CH_2)_2$ -
Glutamine	Gln	Q	$H_2N-CO-(CH_2)_2$ -
Glycine	Gly	G	H -
Histidine	His	H	$NH-CH=N-CH=C-CH_2$ -
Isoleucine	Ile	I	$CH_3-CH_2-CH(CH_3)$ -
Leucine	Leu	L	$(CH_3)_2-CH-CH_2$ -
Lysine	Lys	K	$HN_2-(CH_2)_4$ -
Methionine	Met	M	$CH_3-S-(CH_2)_2$ -
Phenylalanine	Phe	F	$Ph-CH_2$ -
Proline	Pro	P	$(CH_2)_3$ -
Serine	Ser	S	$HO-CH_2$ -
Threonine	Thr	T	$CH_3-CH(OH)$ -
Tryptophan	Trp	W	$Ph-NH-CH=C-CH_2$ -
Tyrosine	Tyr	Y	$HO-Ph-CH_2$ -
Valine	Val	V	$(CH_3)_2-CH$ -

Table S1. Abbreviations and formulas of the 20 common amino acids.

The spike protein used in this study is a recombinant protein of human coronavirus. It is produced with mammalian proteins (particularly, Chinese hamster ovary cells). The purity is more than 90%, which was tested by Sodium Dodecyl Sulfate Polyacrylamide Gel Electrophoresis (SDS-PAGE) analysis. Here, we used a partial domain from 319th to 541st amino acid where receptor-binding domain is located. Molecular weight of this protein fraction is 39 kDa. The primary amino acid sequence of SARS-CoV-2 spike protein 319 Arg to 541 Phe (from Ab cam, catalog number ab27065) is: **RV QPTESIVRFP NITNLCPFGE VFNATRFASV YAWNRKRISN CVADYSVLYN SASFSTFKCY GVSPTKLNDL CFTNVYADSF VIRGDEVRQI APGQTGKIAD YNYKLPDDFT GCVIAWNSNN LDSKVGGNYN YLYRLFRKSN LKPFERDIST EIYQAGSTPC NGVEGFNCYF PLQSYGFQPT NGVGYQPYRV VVLSFELLHA PATVCGPKKS TNVKNKCVN F.**[1]

The primary amino acid sequence of MERS-CoV spike protein 1 Met to 725 Glu (from mybiosource, catalog number MBS434229) is: **SKADGIIYPQ GRTYSNITIT YQGLFPYQGD HGDMYVYSAG HATGTTPQKL FVANYSQDVK QFANGFVVRI GAAANSTGTV IISPSTSATI RKIYPAFMLG SSVGNFSDGK MGRFFNHTLV LLPDGCGTLL RAFYCILEPR SGNHCPAGNS YTSFATYHTP ATDCSDGNYN RNASLNSFKE YFNLRNCTFM YTYNITEDEI LEWFGITQTA QGVHLFSSRY VDLYGGNMFQ FATLPVYDTI KYYSIIPHSI RSIQSDRKAW AAFYVYKLQP LTFLLDFSVD GYIRRAIDCG FNDLSQLHCS YESFDVESGV YSVSSFEAKP SGSVVEQAEG VECDFSPLLS GTPPQVYNFK RLVFTNCNYN LTKLLSLFSV NDFTCSQISP AAIASNCYSS LILDYFSYPL SMKSDLSVSS AGPISQFNYK QSFSNPTCLI LATVPHNLTT ITKPLKYSYI NKCSRLLSDD RTEVPQLVNA NQYSPCVSIV PSTVWEDGDY YRKQLSPLEG GGWLVASGST VAMTEQLQMG FGITVQYGTD TNSVCPKLEF ANDTKIASQL GNCVEYSLYG VSGRGVFQNC TAVGVRQQRF VYDAYQNLVG YYSDDGNYYC LRACVSVPVS VIYDKETKTH ATLFGSVACE HISSTMSQYS RSTRSMLKRR DSTYGPLQTP VGCVLGLVNS SLFVE.**[2]

S2. Raman liquid scans for 2D-band in PBS buffer

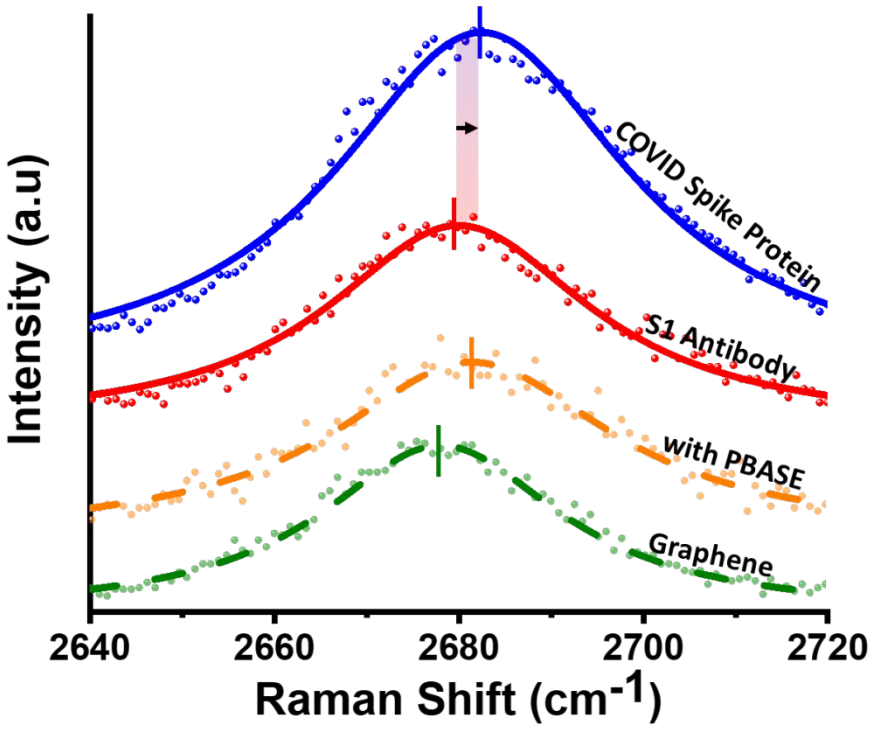

Figure S1. 2D band Raman spectra in liquid (Phosphate buffered saline, pH=7.4) scan of graphene (green), PBASE-modified graphene (orange), graphene-PBASE-Antibody (red), and graphene-PBASE-Antibody-spike protein (blue) structure. While the attachment of PBASE p-dopes, and the antibody n-dopes, the COVID protein attachment p-dopes the device (2D peak upshift by 2.53 $\pm$ 0.35 cm^{-1}). Dots: 2D Raman data points. Lines: Lorentzian fits of the 2D peaks.

The Raman scans were also carried out in Phosphate-buffered saline (PBS) buffer, pH=7.4. The liquid scans showed the same doping effects with the air scans presented in the manuscript. For each process-step: graphene, graphene-PBASE, graphene-PBASE-antibody, and graphene-PBASE-antibody-Spike protein, the structures were interfaced with PBS and Raman spectra were collected on the same spot. Figure S1 shows the representative data of PBS liquid scans for the detection. Graphene's 2D band in PBS (green) has a peak position at 2678.03 cm^{-1}. And the attachment of PBASE showed a blue-shift of 3.42 cm^{-1} (from 2678.03 cm^{-1} to 2681.45 cm^{-1}). The p-doping effect is expected as PBASE withdraws electrons from graphene. The immobilization of antibody on the same area showed a red-shift of 1.51 cm^{-1} (from 2681.45 cm^{-1} to 2679.94 cm^{-1}) as graphene became less p-doped. Finally, protein attachment on the same area showed p-doping effect, with graphene's 2D band position blue-shifting of 2.53 cm^{-1} (from 2679.94 cm^{-1} to 2682.47 cm^{-1}). For the spike protein attachment, the Fermi level change is calculated as: $\Delta E_f = 85.4\, meV$ while the change in p-doping level is estimated as: $\Delta p = 4.4 * 10^{11}$ dopants/cm^2.

S3. Spike protein detection in PBS at low concentrations

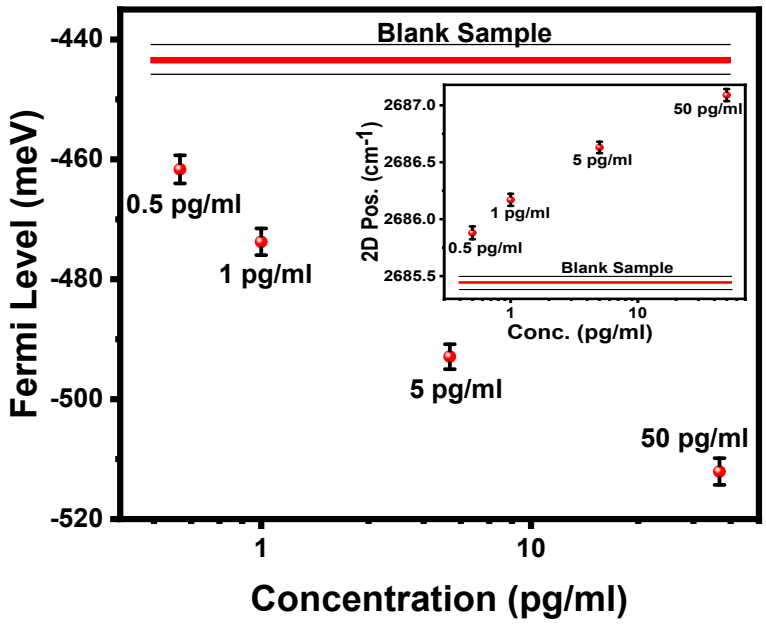

Figure S2. The 2D peak position (inset) and the Fermi level of graphene changes with the concentration of the COVID spike protein (0.5 pg/ml, 1 pg/ml, 5 pg/ml and 50 pg/ml). The response for the blank concentration (0 pg/ml) is also shown.

We provide detection results for low concentrations of 0.5, 1, 5 and 50 pg/ml in Figure S2, in which all scans were conducted on the same area of graphene. The results show an increase in 2D peak position with the higher spike protein concentration. The 2D peak position was at 2685.44 cm^{-1} at the blank sample. This value increases to 2685.88, 2686.17, 2686.63, and 2687.09 cm^{-1} at 0.5 pg/ml, 1 pg/ml, 5 pg/ml, and 50 pg/ml spike protein respectively. Correspondingly, the Fermi level decreases from -443 meV at the blank sample to -462 meV, -474 meV, -493 meV, -512 meV at 0.5 pg/ml, 1 pg/ml, 5 pg/ml, and 50 pg/ml spike protein respectively. The decreasing Fermi level of graphene with higher concentration of CoV-2 S-protein reflects an increase of p-doping due to an increase in protein attachment.

S4. Limit of Detection of SARS-CoV-2 spike protein in PBS

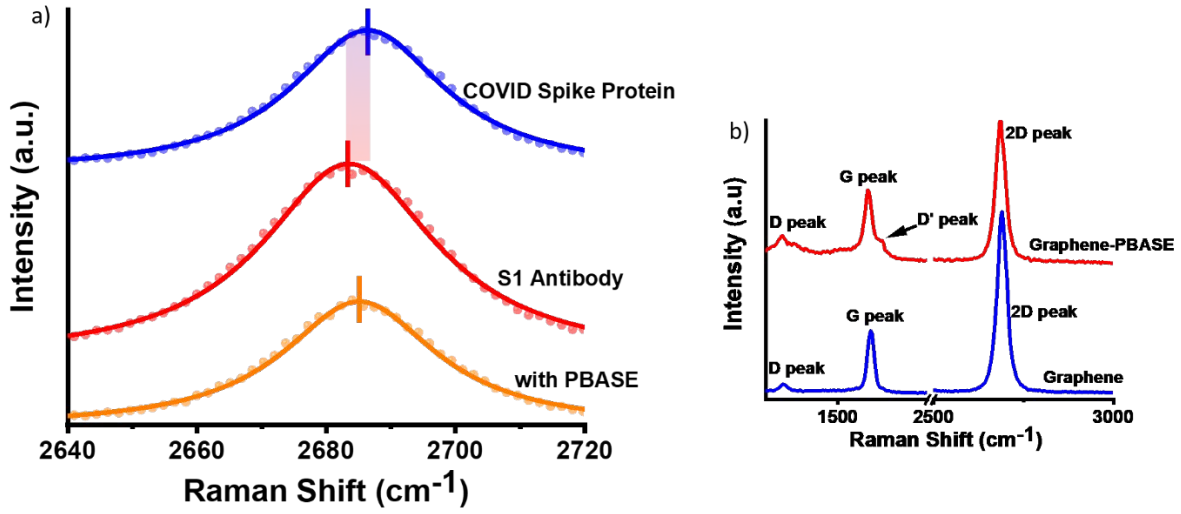

Figure S3. COVID spike protein detection in PBS at 1 fg/ml. (a) The 2D peak of graphene-PBASE (orange), graphene-PBASE-antibody (red), and graphene-PBASE-antibody-Spike Protein (blue) structure are shown. While attachment of antibody n-dopes graphene, the COVID protein p-dopes the devices (2D peak position shifted from 2683.51 cm^{-1} to 2686.41 cm^{-1}). Dots: 2D data-points; Lines: Lorentzian fit of the 2D peak. (b) Representative Raman spectra of the pristine graphene and PBASE-treated graphene. The presence of D' peak and the increase of D peak intensity confirm the attachment of PBASE on graphene.

Consistent with the reported viral load in saliva, sputum, and throat swabs which typically fall in the range of 10^4 – 10^8 copies per ml during the first week of symptoms,[3–5] we tested on our device in PBS with 1 fg/ml, which translates to about 1.544×10^4 copies per ml (Figure S3). The first step of PBASE functionalization on graphene is verified by the presence of D' peak at around 1620 cm^{-1} and the increase in the D peak intensity. On that same spot, the attachment of antibody shifts the 2D-peak position of graphene by 1.6 cm^{-1} from 2685.11 cm^{-1} to 2683.51 cm^{-1} (n-doping). More importantly, the 2D-peak position shift of 2.9 cm^{-1} (from 2683.51 cm^{-1} to 2686.41 cm^{-1}; corresponding to a Fermi level change from -362.9 meV from -483.75 meV) was observed upon the attachment of spike protein (p-doping), which is attributed to the induced-charge carriers caused by the dipole-moment of the attached protein.

The calculation of limit of blank (LOB)[6] and limit of detection (LOD)[6] for two devices tested with 1 fg/ml spike protein solution in PBS is shown below.

a. *Device 1:*

Blank sample (number of different locations tested on the device = 34)

2D peak position average = 2680.33 cm^{-1}; Standard Deviation = 0.46 cm^{-1}.

Low Concentration Sample (number of different locations tested on the device =34)

2D peak position average = 2683.41 cm^{-1}; Standard Deviation = 1.17 cm^{-1}

LOB = 2681.09 cm^{-1}

LOD = 2683.02 cm^{-1}

➔ LOD "Concentration" = 0.87 fg/ml

b. Device 2:

Blank sample (number of different locations tested on the device = 5)

2D peak position average = 2679.30 cm^{-1}; Standard Deviation = 0.68 cm^{-1}.

Low Concentration Sample (number of different locations tested on the device = 5)

2D peak position average = 2681.19 cm^{-1}; Standard Deviation = 1.03 cm^{-1}

LOB = 2680.42 cm^{-1}

LOD = 2682.11 cm^{-1}

➔ LOD "Concentration" = 1.48 fg/ml

S5. Limit of Detection of SARS-CoV-2 spike protein in artificial saliva

Similarly, the calculation of LOB and LOD[6] for low SARS-CoV-2 spike protein concentration in saliva (with 0 fg/ml, 0.5 fg/ml, 1 fg/ml, 3 fg/ml and 4 fg/ml) was also conducted and shown below.

On blank sample (number of different locations tested on the device = 8)

2D peak position average = 2681.18 cm^{-1}; Standard Deviation = 0.54 cm^{-1}.

0.5 fg/ml sample (number of different locations tested on the device = 8)

2D peak position average = 2682.69 cm^{-1}; Standard Deviation = 1.06 cm^{-1}.

1 fg/ml sample (number of different locations tested on the device = 8)

2D peak position average = 2682.7 cm^{-1}; Standard Deviation = 1.75 cm^{-1}.

3 fg/ml sample (number of different locations tested on the device = 8)

2D peak position average = 2683.57 cm^{-1}; Standard Deviation = 0.58 cm^{-1}.

4 fg/ml sample (number of different locations tested on the device = 8)

2D peak position average = 2685.59 cm^{-1}; Standard Deviation = 1.47 cm^{-1}.

The calibration curve is calculated as

$$\frac{[2D\ peak\ position - 2681.654]}{0.878}$$

LOB "Concentration" = 1.018 fg/ml

LOD "Concentration" = 3.75 fg/ml

The calculated limit of detection with saliva sample is ~ 3 fg/ml, which implies a resolution of 4.632×10^4 copies per ml.

S6. Comparison between our work and other detection techniques

The results from our device are compared with other detection techniques in Table S2 below.

Method	Target analyte	Sample type	LOD	Test time (min)	Advantages	Limitations
Protein Based Sensors						
Graphene phononic sensor (**this work**)	Virus spike protein	Respiratory swabs, saliva	25 aM	<1	Potential for real-time detection, low-cost devices, local analysis possible	Spectrometer can be relatively expensive
Biosensors /RDT[7,8]	Virus mRNA /antigen/antibody	Respiratory swabs, buffer	0.2 pM	<1	Real-time detection, quick analysis	High fabrication cost, spectrometer is relatively expensive, Comparatively low accuracy
mRNA Based Sensors						
RT-PCR[9,10]	Virus mRNA	Respiratory swabs, saliva, sputum, BLF	0.15-100 copy/μL	120-140	High sensitivity, specificity, and high throughput	Labor intensive, requires numerous reagents and expensive equipment, accurate results dependent on number of thermal cycles in protocol
CRISPR[11,12]	Virus mRNA	Respiratory swabs, saliva	2-10 copy/μL	45-70	Simple process, low cost, quick turnaround	Risk of contamination
Molecular POC[13–15]	Virus mRNA	Respiratory swabs	0.1-10 copy/μL	13-60	Easy to use, quick results,	Accuracy reduced after symptom begins

Table S2. Comparison with currently available diagnostic tools.

S7. Reduce spike protein non-specific binding by capping unreacted PBASE with glycine

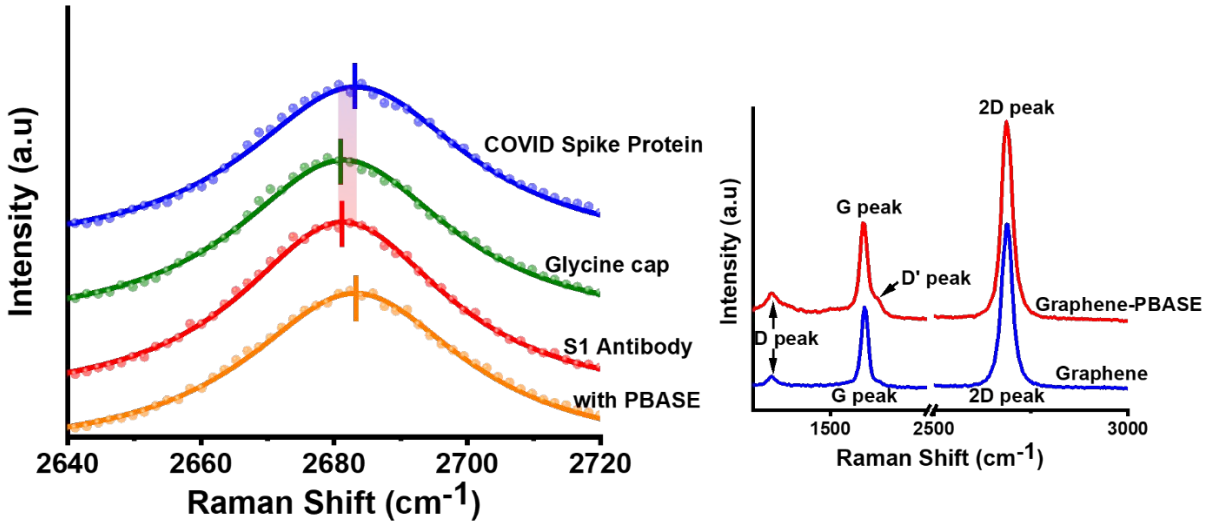

Figure S4. COVID Spike Protein Detection via Graphene Phononics. (Left) The 2D peak of graphene-PBASE (orange), graphene-PBASE-antibody (red), graphene-PBASE-antibody-glycine capped (green) and graphene-PBASE-antibody-glycine capped-Spike Protein (blue) structure are shown. While attachment of the antibody n-dopes graphene, and the glycine shows no change in doping, the COVID protein p-dopes the devices. Dots: 2D data-points; Lines: Lorentzian fit of the 2D peak. (Right) Representative Raman spectra of the pristine graphene and PBASE-treated graphene on the same graphene spot. The presence of D' peak and the increase of D peak intensity confirm the attachment of PBASE on graphene.

Because PBASE has N-hydroxysuccinimide ester group that can react covalently with amine groups in protein molecules, the most active sites for non-specific binding will be the sites with unreacted PBASE on graphene that do not have antibody attached. Therefore, to reduce non-specific binding, we have fabricated devices, where the unfunctionalized PBASE sites have been capped with amine-containing glycine. In Figure S4, all scans were conducted on the same area of graphene. The first step of graphene functionalization with PBASE was verified by the presence of D' peak at around 1620 cm^{-1} and the increase of D peak intensity. On the same spot, the attachment of antibody n-dopes graphene, exhibiting a 2D peak position shift of 1.84 cm^{-1} (from 2683.18 cm^{-1} to 2681.34 cm^{-1}). Afterward, the structure was incubated in glycine solution to cap unreacted PBASE. The 2D peak on that same area shows practically no shift after glycine attachment (from 2681.34 cm^{-1} to 2681.43 cm^{-1}, which is within the error range). Finally, the spike protein attachment shows p-doping with a 2D peak shift of 1.85 cm^{-1} (from 2681.43 cm^{-1} to 2683.28 cm^{-1}), which is attributed to induce-charge carriers caused by protein potential.

S8. Voltage calculation

$$n_T = 6 \times 10^7 \times (-242.3)^2 \times 10^4 = 3.5 \times 10^{16} \frac{dopant}{m^2}$$

$$C_Q = \frac{4e^2\sqrt{\pi}}{hv_F}\sqrt{n_T} = \frac{4 \times (1.6 \times 10^{-19})^2 \times \sqrt{3.14}}{(6.63 \times 10^{-34}) \times 10^6} \times \sqrt{(3.5 \times 10^{16})} \left[\frac{C^2}{(J.s).(m.s^{-1})}\sqrt{\frac{dopant}{m^2}}\right]$$
$$= (5.14 \times 10^{-2}) \ [F.m^{-2}]$$

$$Q = (4.1 \times 10^{15}) \times (1.6 \times 10^{-19})\left[\frac{dopant}{m^2} * C\right] = (6.6 \times 10^4) \ [C.m^{-2}]$$

$$V = \frac{Q}{C_Q} = \frac{6.6 \times 10^4}{5.14 \times 10^{-2}}\left[\frac{C.m^{-2}}{F.m^{-2}}\right] = 1.28 \times 10^{-2} \ [V] = 12.8 \ [mV]$$

S9. Regression error

The error-values for the 2D peak position and the Fermi level are provided in the table below. These errors are calculated as the regression-error from fitting the Lorentz model from an average of 3000 spectra (with each spectrum containing 1024 wavenumber-points) for each of the sample concentrations. Representative regression error (shown in the table below) for the 2D peak position varies from 0.05 to 0.06271 cm^{-1}, and the corresponding values for the Fermi level ranges from 2.0865 to 2.613 meV.

	2D peak position	Regression error	Fermi Level (Ef)	Regression error
	Unit: cm^{-1}		Unit: meV	
Antibody	2685.44	0.06271	-443.333	2.613
0.5 pg/ml	2685.88	0.05626	-461.667	2.3445
1 pg/ml	2686.17	0.05335	-473.75	2.223
5 pg/ml	2686.63	0.05007	-492.917	2.0865
50 pg/ml	2687.09	0.05339	-512.083	2.2245

S10. Graphene grain size estimation

The quality of graphene's crystallinity is very important and can be measured by Raman.[16] Here the crystal size (La) can be calculated by $La = {}^{490}\Big/\left(\left({}^{I_D}\Big/_{I_G}\right)E_L^4\right) nm$ (E_L = 2.33 eV (532 nm)).

This gives a crystal size of 415 nm for our samples. This will mean that in the experiments conducted with a spot size of 721 nm, there will be a few grain boundaries.

S11. XPS analysis of the antibody attachment

Atomic percentage and the number of each element (with 100 silicone atoms) in 4 samples: SiO_2 substrate, Graphene, Graphene-PBASE, and Graphene-PBASE-Antibody are shown in the tables below:

Unit (%)	Substrate (SiO_2)	Graphene	Graphene-PBASE	Graphene-PBASE-Antibody
Si 2p	32.25%	27.05%	26.45%	13.41%
O 1s	62.90%	52.81%	41.67%	26%
C 1s	4.85%	19.96%	30.44%	50.26%
N 1s		0.18%	1.45%	10.33%

Unit (atoms)	Substrate (SiO_2)	Graphene	Graphene-PBASE	Graphene-PBASE-Antibody
Si 2p	100	100	100	100
O 1s	195.04	195.23	157.54	193.89
C 1s	15.04	73.79	115.09	374.79
N 1s		0.67	5.48	77.03
C added		58.75	41.30	259.71
N added			4.82	71.55

Table S3: Elemental composition from XPS for SiO2, graphene, graphene-PBASE, and graphene-PBASE-Ab

$$\frac{N_{Antibody}}{C_{Antibody}} = \frac{71.55}{259.71} = \mathbf{0.275}$$

From the table, we estimate the antibody density:

$$\frac{Carbon\ Graphene}{Silicone} = \frac{C_{Graphene}}{Si_{Graphene}} - \frac{C_{Si}}{Si_{Si}} = \frac{19.96\%}{27.05\%} - \frac{4.85\%}{32.25\%} = 0.588$$

$$\frac{Nitrogen}{Silicone} = \frac{N_{Antibody}}{Si_{Antibody}} - \frac{N_{PBASE}}{Si_{PBASE}} = \frac{10.33\%}{13.41\%} - \frac{1.45\%}{26.45\%} = 0.716$$

$$\frac{Nitrogen}{Carbon\ Graphene} = \frac{Nitrogen}{Silicone} \div \frac{Carbon\ Graphene}{Silicone} = 0.716 \div 0.588 = 1.218$$

We know that 1 nm^2 of graphene has 38.46 carbon atoms. From that, on 1 nm^2 of graphene, the number of nitrogen atoms is

$$\frac{Nitrogen}{Carbon\ Graphene} \times Carbon\ Graphene = 1.218 \times 38.46 = 46.84\ \frac{Nitrogen\ atom}{nm^2}$$

Because one antibody has about 333 nitrogen atoms, the antibody density is

$$46.84\,\frac{Nitrogen\ atom}{nm^2}\times\frac{10^6\,nm^2}{1\,\mu m^2}\times\frac{1\,antibody}{333\,Nitrogen\ atom}=140{,}661\,\frac{antibodies}{\mu m^2}$$

References

(1) UniProtKB - P0DTC2 (SPIKE_SARS2). https://www.uniprot.org/uniprot/P0DTC2 (accessed May 29, 2021).

(2) UniProtKB - R9UQ53 (R9UQ53_MERS). https://www.uniprot.org/uniprot/R9UQ53 (accessed May 29, 2021).

(3) To, K. K. W.; Tsang, O. T. Y.; Leung, W. S.; Tam, A. R.; Wu, T. C.; Lung, D. C.; Yip, C. C. Y.; Cai, J. P.; Chan, J. M. C.; Chik, T. S. H.; Lau, D. P. L.; Choi, C. Y. C.; Chen, L. L.; Chan, W. M.; Chan, K. H.; Ip, J. D.; Ng, A. C. K.; Poon, R. W. S.; Luo, C. T.; Cheng. V. C. C.; *et al.* Temporal Profiles of Viral Load in Posterior Oropharyngeal Saliva Samples and Serum Antibody Responses during Infection by SARS-CoV-2: An Observational Cohort Study. *Lancet Infect. Dis.* **2020**, *20*, 565–574.

(4) Zhu, J.; Guo, J.; Xu, Y.; Chen, X. Viral Dynamics of SARS-CoV-2 in Saliva from Infected Patients. *J. Infect.* **2020**, *81*, e48–e50.

(5) Pan, Y.; Zhang, D.; Yang, P.; Poon, L. L. M.; Wang, Q. Viral Load of SARS-CoV-2 in Clinical Samples. *Lancet Infect. Dis.* **2020**, *20*, 411–412.

(6) Armbruster, D. A.; Pry, T. Limit of Blank, Limit of Detection and Limit of Quantitation. *Clin. Biochem. Rev.* **2008**, *29 Suppl 1*, S49-52.

(7) Qiu, G.; Gai, Z.; Tao, Y.; Schmitt, J.; Kullak-Ublick, G. A.; Wang, J. Dual-Functional Plasmonic Photothermal Biosensors for Highly Accurate Severe Acute Respiratory Syndrome Coronavirus 2 Detection. *ACS Nano* **2020**, *14*, 5268–5277.

(8) Seo, G.; Lee, G.; Kim, M. J.; Baek, S.-H.; Choi, M.; Ku, K. B.; Lee, C.; Jun, S.; Park, D.; Kim, H. G.; Kim, S.-J. S. I. S.; Lee, J.; Kim, B. T.; Park, E. C.; Kim, S.-J. S. I. S. Rapid Detection of COVID-19 Causative Virus (SARS-CoV-2) in Human Nasopharyngeal Swab Specimens Using Field-E Ff Ect Transistor- Based Biosensor. *ACS Nano* **2020**.

(9) Corman, V. M.; Landt, O.; Kaiser, M.; Molenkamp, R.; Meijer, A.; Chu, D. K. W.; Bleicker, T.; Brünink, S.; Schneider, J.; Schmidt, M. L.; Mulders, D. G. J. C.; Haagmans, B. L.; Van Der Veer, B.; Van Den Brink, S.; Wijsman, L.; Goderski, G.; Romette, J. L.; Ellis, J.; Zambon, M.; Peiris, M.; *et al.* Detection of 2019 Novel Coronavirus (2019-NCoV) by Real-Time RT-PCR. *Eurosurveillance* **2020**, *25*.

(10) Vogels, C. B. F.; Brito, A. F.; Wyllie, A. L.; Fauver, J. R.; Ott, I. M.; Kalinich, C. C.; Petrone, M. E.; Casanovas-Massana, A.; Catherine Muenker, M.; Moore, A. J.; Klein, J.; Lu, P.; Lu-Culligan, A.; Jiang, X.; Kim, D. J.; Kudo, E.; Mao, T.; Moriyama, M.; Oh, J. E.; Park, A.; *et al.* Analytical Sensitivity and Efficiency Comparisons of SARS-CoV-2 RT–QPCR Primer–Probe Sets. *Nat. Microbiol.* **2020**, *5*, 1299–1305.

(11) Broughton, J. P.; Deng, X.; Yu, G.; Fasching, C. L.; Servellita, V.; Singh, J.; Miao, X.; Streithorst, J. A.; Granados, A.; Sotomayor-Gonzalez, A.; Zorn, K.; Gopez, A.; Hsu, E.; Gu, W.; Miller, S.; Pan, C. Y.; Guevara, H.; Wadford, D. A.; Chen, J. S.; Chiu, C. Y. CRISPR–Cas12-Based Detection of SARS-CoV-2. *Nat. Biotechnol.* **2020**, *38*, 870–874.

(12) Hou, T.; Zeng, W.; Yang, M.; Chen, W.; Ren, L.; Ai, J.; Wu, J.; Liao, Y.; Gou, X.; Li, Y.;

Wang, X.; Su, H.; Gu, B.; Wang, J.; Xu, T. Development and Evaluation of a Rapid CRISPR-Based Diagnostic for COVID-19. *PLoS Pathog.* **2020**, *16*, 1–12.

(13) Joung, J.; Ladha, A.; Saito, M.; Segel, M.; Bruneau, R.; Huang, M. L. W.; Kim, N. G.; Yu, X.; Li, J.; Walker, B. D.; Greninger, A. L.; Jerome, K. R.; Gootenberg, J. S.; Abudayyeh, O. O.; Zhang, F. Point-of-Care Testing for COVID-19 Using SHERLOCK Diagnostics. **2020**, 10.1101/2020.05.04.20091231. medRXiv. https://www.medrxiv.org/content/10.1101/2020.05.04.20091231v1 (accessed May 29, 2021).

(14) Carter, L. J.; Garner, L. V.; Smoot, J. W.; Li, Y.; Zhou, Q.; Saveson, C. J.; Sasso, J. M.; Gregg, A. C.; Soares, D. J.; Beskid, T. R.; Jervey, S. R.; Liu, C. Assay Techniques and Test Development for COVID-19 Diagnosis. *ACS Cent. Sci.* **2020**, *6*, 591–605.

(15) Xue, G.; Li, S.; Zhang, W.; Du, B.; Cui, J.; Yan, C.; Huang, L.; Chen, L.; Zhao, L.; Sun, Y.; Li, N.; Zhao, H.; Feng, Y.; Wang, Z.; Liu, S.; Zhang, Q.; Xie, X.; Liu, D.; Yao, H.; Yuan, J. Reverse-Transcription Recombinase-Aided Amplification Assay for Rapid Detection of the 2019 Novel Coronavirus (SARS-CoV-2). *Anal. Chem.* **2020**, *92*, 9699–9705.

(16) Ribeiro-Soares, J.; Oliveros, M. E.; Garin, C.; David, M. V.; Martins, L. G. P.; Almeida, C. A.; Martins-Ferreira, E. H.; Takai, K.; Enoki, T.; Magalhães-Paniago, R.; Malachias, A.; Jorio, A.; Archanjo, B. S.; Achete, C. A.; Cançado, L. G. Structural Analysis of Polycrystalline Graphene Systems by Raman Spectroscopy. *Carbon N. Y.* **2015**, *95*, 646–652.